Atmos. Chem. Phys., 14, 5943–5957, 2014
www.atmos-chem-phys.net/14/5943/2014/
doi:10.5194/acp-14-5943-2014

Atmospheric Chemistry and Physics
Open Access

Developing a western Siberia reference site for tropospheric water vapour isotopologue observations obtained by different techniques (in situ and remote sensing)

K. Gribanov[1], J. Jouzel[2], V. Bastrikov[1,2,3], J.-L. Bonne[2], F.-M. Breon[2], M. Butzin[4], O. Cattani[2], V. Masson-Delmotte[2], N. Rokotyan[1], M. Werner[4], and V. Zakharov[1]

[1]Climate and Environmental Physics Laboratory, Ural Federal University, Yekaterinburg, Russia
[2]Institut Pierre Simon Laplace, Laboratoire des Sciences du Climat et de l'Environnement, Gif-sur-Yvette, France
[3]Institute of Industrial Ecology UB RAS, Yekaterinburg, Russia
[4]Alfred Wegener Institute for Polar and Marine Research, Bremerhaven, Germany

Correspondence to: K. Gribanov (kgribanov@remotesensing.ru)

Received: 2 January 2013 – Published in Atmos. Chem. Phys. Discuss.: 24 January 2013
Revised: 31 March 2014 – Accepted: 25 April 2014 – Published: 16 June 2014

Abstract. Water stable isotopologues provide integrated tracers of the atmospheric water cycle, affected by changes in air mass origin, non-convective and convective processes and continental recycling. Novel remote sensing and in situ measuring techniques have recently offered opportunities for monitoring atmospheric water vapour isotopic composition. Recently developed infrared laser spectrometers allow for continuous in situ measurements of surface water vapour δD_v and $\delta^{18}O_v$. So far, very few intercomparisons of measurements conducted using different techniques have been achieved at a given location, due to difficulties intrinsic to the comparison of integrated with local measurements. Nudged simulations conducted with high-resolution isotopically enabled general circulation models (GCMs) provide a consistent framework for comparison with the different types of observations. Here, we compare simulations conducted with the ECHAM5-wiso model with two types of water vapour isotopic data obtained during summer 2012 at the forest site of Kourovka, western Siberia: hourly ground-based FTIR total atmospheric columnar δD_v amounts, and in situ hourly Picarro δD_v measurements. There is an excellent correlation between observed and predicted δD_v at surface while the comparison between water column values derived from the model compares well with FTIR estimates.

1 Introduction

Owing to slight differences in the saturation vapour pressure and diffusivity in air of $H_2^{16}O$, $HD^{16}O$ and $H_2^{18}O$ molecules, fractionation processes occur during phase changes of the water. As a result, the distribution of the water isotopologues (hereafter δD and $\delta^{18}O$ expressed in ‰ vs. Vienna Standard Mean Ocean Water (VSMOW); Craig, 1961) varies both spatially and temporally in the atmospheric water vapour and in the precipitation. Until recently, our knowledge of their present-day distribution has focused on precipitation, much easier to sample than atmospheric water vapour. This sampling difficulty partly explains why applications dealing with studies of atmospheric processes and atmospheric dynamics have long been limited while they have rapidly developed in such fields as isotope hydrology and isotope palaeoclimatology (from ice cores and other archives).

The situation has recently changed thanks to technological advances which now allow for either in situ measurement of δD_v and $\delta^{18}O_v$ or remote estimation of δD_v in atmospheric water vapour. The quantification of water isotopologues in tropospheric water vapour based on space-based remote sensing techniques pioneered by Zakharov et al. (2004) is now under rapid development (J. Worden et al., 2006; Payne et al., 2007; Nassar et al., 2007; Steinwagner et al., 2007; Frankenberg et al., 2009, 2012; Schneider and Hase , 2011; Herbin et al., 2009; Field et al., 2013; Lacour et al., 2012; Boesch et al., 2013) and provides large-scale,

integrated measurements. Data from ground-based high-resolution Fourier transform infrared (FTIR) spectrometers have been exploited to retrieve information about vertical profiles of water stable isotopologues (mainly δD_v) in water vapour from instruments both from the NDACC (Network for the Detection of Atmospheric Composition Change) sites (Schneider et al., 2006, 2010a, b, 2012) and columnar δD_v values from the TCCON (Total Carbon Column Observing Network) network (Boesch et al., 2013; Risi et al., 2012a).

A third major breakthrough has been accomplished with new infrared (IR) laser spectrometers reaching the same level of precision as mass spectrometers, and becoming commercially available (Brand, 2009; Gupta et al., 2009). These devices are sufficiently robust to allow field measurements of the δD_v and $\delta^{18}O_v$ composition of water vapour. After the development of calibration protocols, which require the introduction of reference waters and corrections for humidity and instrumental drift, such instruments have been deployed from tropical (Tremoy et al., 2012) to polar locations (Steen-Larsen et al., 2011) where they have revealed significant diurnal to seasonal variability in relationship with air mass origins, convection and surface–atmosphere moisture fluxes. Prior to the deployment of a network of stations where the δD_v and $\delta^{18}O_v$ of surface water vapour will be continuously monitored, the information brought by water vapour stable isotopologues must be assessed for different climatic conditions.

In parallel, our ability to describe and simulate the distribution of water isotopologues using atmospheric general circulation models in which fractionation processes are embedded (IGCMs) has made considerable progress since the pioneering studies conducted in the 1980s (Joussame et al., 1984; Jouzel et al., 1987). High-resolution atmospheric models can now be nudged to atmospheric analysis products, allowing for precise comparisons with measurements in a consistent large-scale meteorological framework. Sensitivity studies to uncertain atmospheric model parameterizations have shown the potential of water vapour isotopic data to constrain the representation of key processes linked to for example cloud microphysics (Schmidt et al., 2005) or convection (Risi et al., 2012a).

In a comprehensive approach, Risi et al. (2012a, b) have brought together and compared satellite data sets from various instruments (SCIAMACHY, TES, ACE and MIPAS) and ground-based remote sensing (FTIR at the NDACC and TCCON sites) and in situ techniques (surface vapour measurements and in situ aircraft data). From this comparison Risi et al. (2012a) extracted the most robust features and then used the LMDZ IGCM (LMDZiso) to understand and quantify the sources of differences between these data sets. They pointed out significant differences between data sets but their common features appear to be remarkably well reproduced by LMDZiso in the lower and mid-troposphere, at large scale. However, in Risi et al. (2012a), the amplitude of seasonal variations, the meridional isotopic gradient and the contrast between dry and convective tropical regions were underestimated by LMDZiso as well as by six other IGCMs involved in the SWING2 (Stable Water INtercomparison Group phase 2) intercomparison project.

Such data model intercomparison is a prerequisite if we want to use the variety of information on isotopic distribution in atmospheric water vapour (satellite data, ground-based and in situ measurements) to diagnose biases in the representation of atmospheric processes in general circulation models (GCMs) or infer information about e.g. continental recycling. In their approach Risi et al. (2012b) aimed to use all available isotopic information with the consequence that the various data sets do not cover the same periods and the same locations, a difficulty which however is largely circumvented by applying a rigorous model–data comparison methodology.

Here, we propose a complementary approach which consists in focusing on one site, the Kourovka Observatory (near Yekaterinburg, close to the western boundary of western Siberia, 57.038° N, 59.545° S, see Fig. 1). This site is characterized by a well-marked continental climate, with monthly mean temperatures varying from $-16\,^{\circ}C$ (January) to $+17\,^{\circ}C$ (July) and about 460 mm of annual precipitation, peaking in summer. It is affected by different air mass trajectories and summer continental precipitation recycling (Shalaumova et al., 2010). Its position in a pristine peatland and near the permafrost zone is strategic for the monitoring of the coupling between surface water and carbon budgets. At this site, we have access both to ground-based (FTIR) and in situ vapour measurements (PICARRO L2130-i instrument). Comparison between different sets of δD have been performed before – Lossow et al. (2011) compared between retrievals from different satellite sensors (Envisat/MIPAS, Odin/SMR, SCISAT/ACE-FTS), Schneider and Hase (2011) compared IASI and NDACC FTIR retrievals, Boesch et al. (2013) compared GOSAT short-wave infrared and TCCON FTIR retrievals, and Worden et al. (2011) compared TES retrievals with in situ measurements. Here, we intercompare two independent data sources (PICARRO and FTIR) using the outputs of the ECHAM5-wiso isotopic AGCM (T63) that has been run in a nudged version using ERA-Interim reanalysis fields (Dee et al., 2011; Berrisford et al., 2009). This intercomparison will focus on a relatively short period between April and September 2012.

2 In situ isotopic measurements of surface water vapour

A Picarro laser instrument of type L2130-i was received by Ural Federal University in March 2012. Laboratory tests and further periodic calibration in the field were conducted in order to verify the reproducibility of the device using two different reference water samples: (i) DW (distilled water with $\delta D = -96.4\,‰$); (ii) YEKA (mixing Antarctic snow

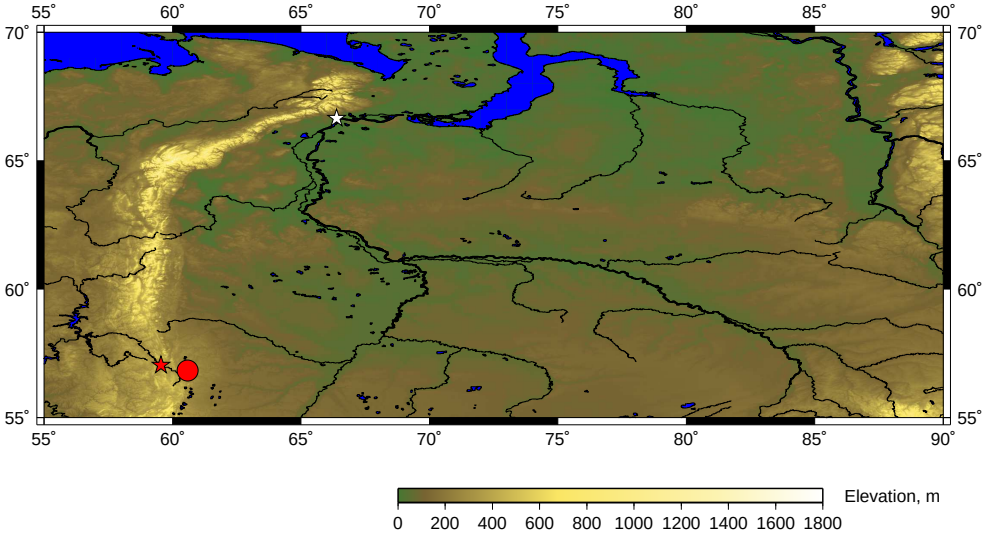

Figure 1. Map of the target region (western Siberia). Kourovka observation site is marked with a red star and Yekaterinburg is marked with a red circle. The white star denotes the future site at Labytnangi.

with distilled water with $\delta D = -289.0$ ‰). A third depleted reference sample (iii) DOMEC (LSCE water standard with $\delta D = -424.1$ ‰) was also used to assess the linearity of the system. Exact isotopic values of the reference water samples were measured at LSCE by IRMS.

The instrument was installed in Kourovka Observatory in mid-March 2012, inside the same room as the FTIR spectrometer. Also the Kourovka site is equipped with Gill Instruments MetPak-II meteorological station which provides every second measurements of atmospheric pressure, wind speed and direction, air temperature and relative humidity.

The quality of the post-processed data strongly depends on the stability of the calibrations. Water standard measurements are considered unstable and not taken into account when standard deviations of humidity and δD_v are above 600 ppm and 3 ‰, respectively. During the measurement period (from April to September) the total number of successful calibrations was 70 for DW and 130 for YEKA.

Figure 2 shows the variability in the measured standards fitted with polynomial of fifth degree. Despite the presence of certain gaps in calibrations due to the problems with power supply, leakage of SDM syringe and instability of SDM software, the overall drift of the system during 6 months is less than 5 ‰. Fitted polynomials were used for transferring the instrument isotopic values to the V-SMOW scale.

As outlined by Steen-Larsen et al. (2013), isotopic measurements are sensitive to water vapour concentration, so it is required to establish calibration response functions as a function of humidity, based on measurement of reference waters injected at different humidity levels, from 1000 to 25 000 ppm. These response functions were determined in situ in April 2012. However, for the period of interest we do not observe any significant effect on the measured δD_v values. Humidity level changes from 5000 to 29 000 ppm with the mean value of 14 000 ppm and this leads to variation in humidity–isotopologue of response less than 3 ‰.

The overall calibration protocol used was realized according to the six-step protocol described in Steen-Larsen et al. (2013), except for the humidity correction that was not applied for this case.

Finally, we use both hourly and daily average values to present this data set and compare it with ECHAM5-wiso model results. For the period from 1 April to 30 September 2012 over which we will compare data and model results, 2476 hourly PICARRO measurements were produced which corresponds to 67 % of the total duration (3671 h). As FTIR (Sect. 4) data are specifically used to get information about δD_v in the water column, we will hereafter focus on this parameter both for the discussion of the data set and its comparison with model results.

The currently available δD_v data set extends to 21 November. We have, in Fig. 3, displayed both hourly individual measurements and a smooth curve (five-point running mean) limited to periods over which there are at least 6 hourly measurements successively. The amount of water vapour (as measured by the PICARRO instrument) is reported in the same figure along with surface temperature using either measurements at the site available since 1 April or ERA-Interim reanalysis data for the entire period (as used for the simulation).

As expected, the deuterium time series shows a clear seasonal cycle with its lowest values in spring (minimum −232 ‰ on 5 April) and in autumn (minimum −246 ‰ on 18 November) and highest levels during summer (−103 ‰ reached on 14 July and 11 August). While the highest monthly mean values are observed in June–August, the

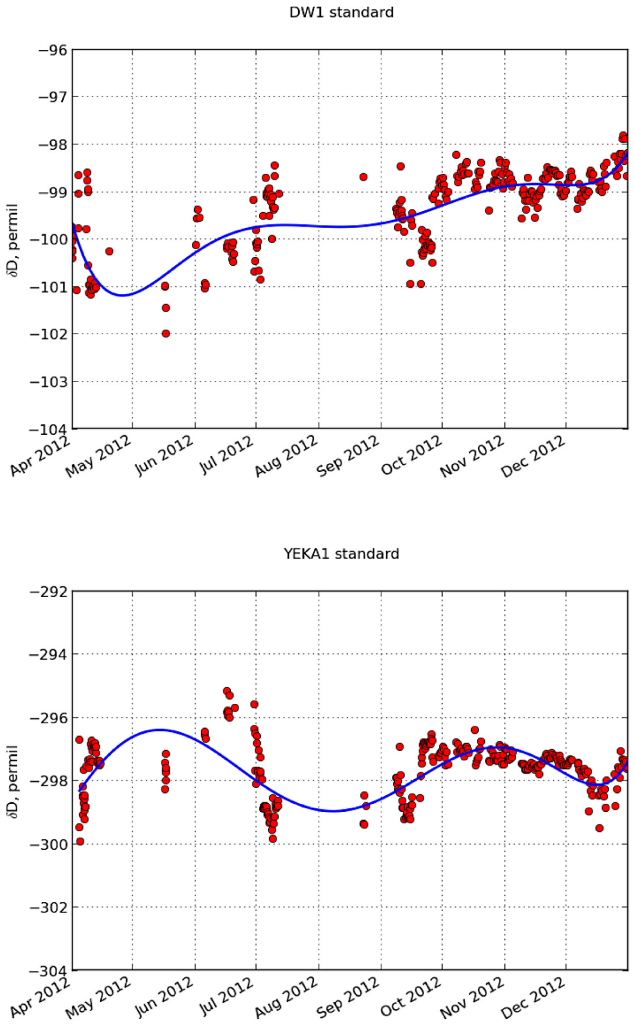

Figure 2. Variability of DW1 (top panel) and YEKA1 (bottom panel) standards measurements along with the polynomial fit used for calibration.

highest single hourly value is recorded to occur in spring (−92 ‰ on 10 May). Indeed, large, and for some of them, rapid δD_v variations are superimposed on this seasonal cycle which will be fully described when winter data are available. These fluctuations are more pronounced in autumn with amplitudes reaching about 100 ‰ than during the summer during which no fluctuation exceeds 45 ‰. They are clearly related to large variations in temperature and to associated changes in the amount of water vapour, q_v.

Although much too simplistic, a Rayleigh type model helps to understand this link between δD_v, temperature and q_v. This model (Dansgaard, 1964) considers the isotopic fractionation occurring in an isolated air parcel in which the condensed phase is assumed to form in isotopic equilibrium with the surrounding vapour and to be removed immediately from the parcel. The isotopic composition of the water vapour at a given site, δD_v, is well approximated by

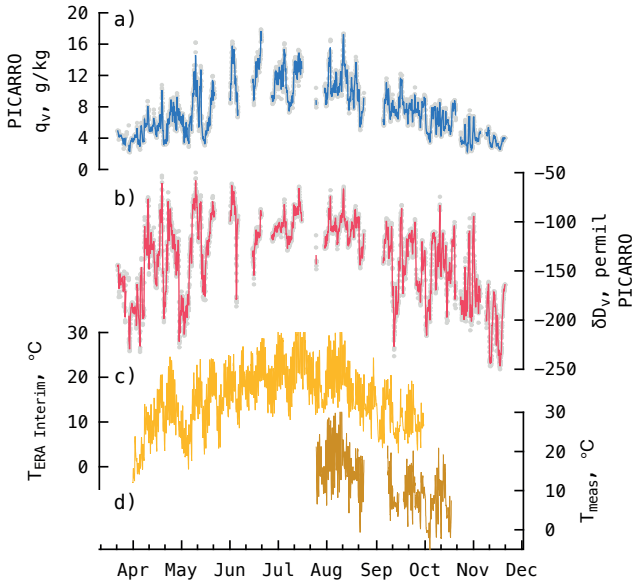

Figure 3. Time series including **(a)** hourly (grey dots) and running (five-point, blue curve) means of specific humidity measured by PICARRO at Kourovka station, **(b)** hourly (grey dots) and running (five-point, red curve) means of δD measured by PICARRO at Kourovka, **(c)** local temperature derived from ERA-Interim reanalysis data, **(d)** local temperatures measured at Kourovka by MetPak-II meteorological station.

$\delta D_v = \left((1+\delta D_0)(q_v/q_0)^{(\alpha_m-1)}\right) - 1$, in which δD_0 and q_0 are the deuterium content and the amount of water vapour at the oceanic origin of the air mass, while α_m stands for the average value of the fractionation coefficient between the oceanic source and the sampling site. Assuming no change in the conditions prevailing at the oceanic source (which again is too simplistic) this should translate into a linear relationship between $\ln(1+\delta D_v)$ and $\ln(q_v)$ while the link with site temperature results from the Clausius–Clapeyron equation.

With this in mind, we have plotted $\ln(1+\delta D_v)$ vs. $\ln(q_v)$ hourly (Fig. 4a) and daily (Fig. 4b) means and δD_v vs. the site temperature using either hourly data for the period over which we have measurements at the site (Fig. 4c) or daily temperature in the Kourovka grid box (Fig. 4d) as derived from reanalysis data (see Sect. 4.1). In line with the Rayleigh model in which the fraction of water remaining in the cloud is the primary driver of isotopic changes, there is a strong correlation ($r^2 = 0.67$) between $\ln(1+\delta D_v)$ and $\ln(q_v)$ for hourly data which increases ($r^2 = 0.71$) when considering daily data and thus eliminating the diurnal cycle. The correlation of δD_v with temperature is weaker for hourly data either using local meteorological measurements ($r^2 = 0.46$) or reanalysis data ($r^2 = 0.49$, not shown). It increases for daily data ($r^2 = 0.72$) at a similar level as observed for $\ln(q_v)$.

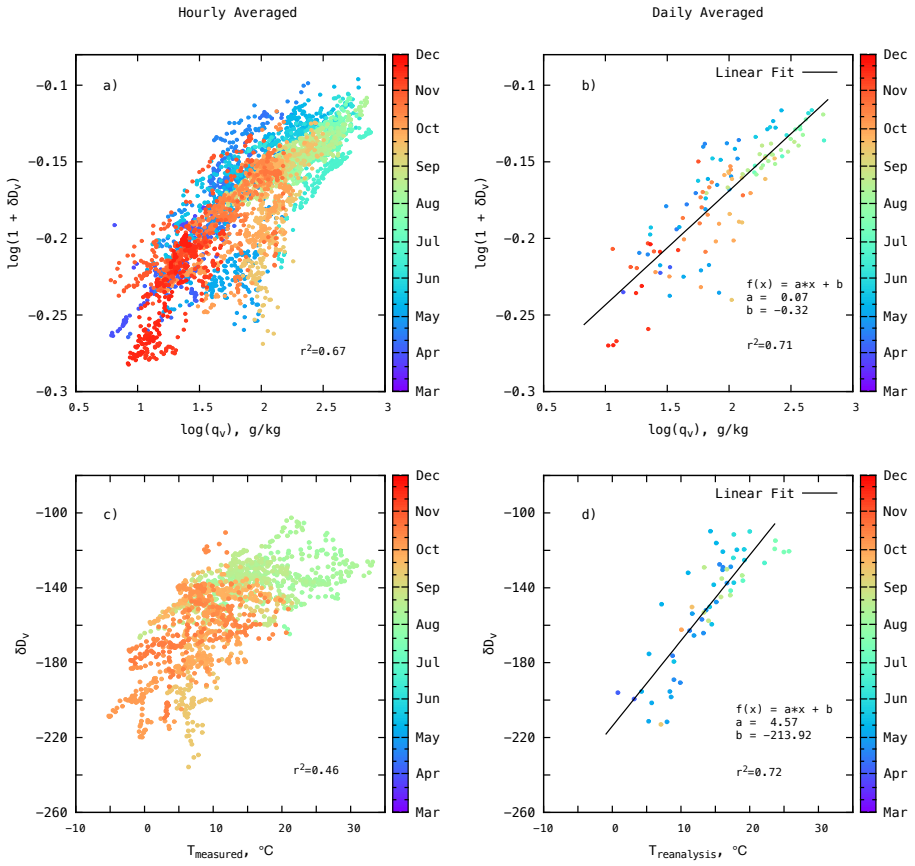

Figure 4. Scatter plots for $\ln(1+\delta D_v)$ vs. $\ln(q_v)$, hourly **(a)** and daily **(b)** means; δD_v (PICARRO) vs. local temperature measured at Kourovka **(c)**; δD_v (PICARRO) vs. ERA-Interim reanalysis temperatures **(d)**.

3 Ground-Based FTIR

Ground-based FTIR spectrometers are widely used for remote measurements of the atmospheric composition (Notholt and Scherms, 1994; Wunch et al., 2010, 2011; Hannigan et al., 2009). Data from the Ural Atmospheric Fourier Station (UAFS) in Kourovka astronomical observatory (57.048° N, 59.545° W, 270 m altitude, 80 km to the west from Yekaterinburg city) were used for comparison with ECHAM5-wiso output. UAFS provides high-resolution ground-based observations of atmospheric transmittance in the spectral region of 4000–11 000 cm^{-1}. At TCCON sites, operating instruments are Bruker IFS-120HR and IFS-125HR (Wunch et al., 2010, 2011) which provide accurate and precise retrieval of column-averaged atmospheric concentrations of such gases as CO_2, CH_4, H_2O, HDO, etc. UAFS is equipped with a Bruker IFS-125M mobile spectrometer (aligned by TCCON members in July 2012). At present, TCCON does not accept mobile versions of IFS-125 instruments but some studies show that they are able to achieve the required accuracy and precision ($< 0.20\%$ for XCO_2, and $< 0.16\%$ for XCH_4) (Petri, 2012).

Columnar values of δD_v^{FTIR} were derived from total column abundances of HDO and H_2O retrieved from the spectra recorded from July 2012 to June 2013 in Kourovka. For data processing, the standard TCCON software GFIT was used (Wunch et al., 2010, 2011). GFIT retrieves the total number of molecules in the vertical atmospheric column, using the algorithm of profile scaling retrieval with the assumption that the shape of the profile of the retrieved gas is well known. H_2O, temperature and pressure a priori profiles are based on reanalysis data provided by National Centers for Environmental Prediction and the National Center for Atmospheric Research (NCEP/NCAR) (Kalnay et al., 1996). The HDO a priori profile is calculated from the H_2O profile as follows (Wunch et al., 2011):

$$x_{HDO}^{apr} = 0.16 x_{H_2O}^{apr} \left(8.0 + \log_{10}\left(x_{H_2O}^{apr}\right)\right) \quad (1)$$

where x_{HDO}^{apr} is the a priori HDO volume mixing ratio (VMR) profile, and $x_{H_2O}^{apr}$ is the a priori H_2O VMR profile. Examples for H_2O and corresponding δD_v^{FTIR} a priori profiles obtained from NCEP reanalysis data for each day of July 2012 are shown in Fig. 9. Most of the δD variations are already represented in a priori vertical profiles (see Fig. 10). HDO

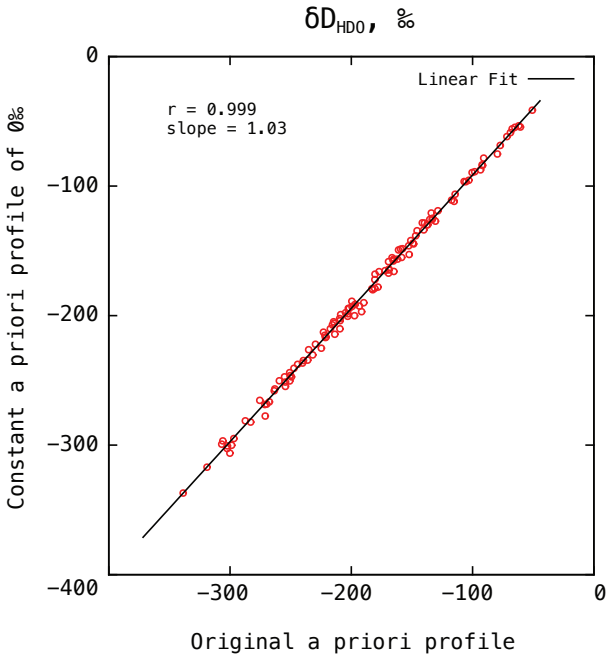

Figure 5. Sensitivity of the retrieval from FTIR observations to different a priori assumptions. Retrievals started from initial guess defined by Eq. (1) are plotted vs. retrievals started from constant and equal to zero initial guess δD_v vertical profile. Standard deviation of retrieval difference is about 1 ‰.

signatures in the near-infrared spectral region are rather weak compared to the H_2O signatures. The informational content of such measurements is discussed in Sect. 5.2. Microwindows containing saturated H_2O lines were excluded from final results to achieve more robust retrieval. As database of water vapour spectral parameters, the revised line list was used (Shillings et al., 2011). Spectral parameters of other gases were taken from the HITRAN 2008 line list (Rothman et al., 2009). To check the sensitivity of the retrieval to the a priori vertical profile of HDO, another retrieval run with constant δD_v a priori profile equal to zero (corresponding to natural abundance of HDO in the ocean) was performed. Figure 5 shows a scatter plot for δD_v values retrieved using different a priori vertical profiles. This reveals that the retrieval of columnar δD_v values does not depend essentially on the initial guess.

4 The ECHAM isotopic model

4.1 Model setup

Atmospheric simulations were carried out using ECHAM5-wiso (Werner et al., 2011), which is the isotopologue-enhanced version of the atmospheric general circulation model ECHAM5 (Roeckner et al., 2003, 2006; Hagemann et al., 2006). Both stable water isotopologues $H_2^{18}O$ and HDO have been explicitly implemented into its hydrological cycle (Werner et al., 2011) analogous to the isotope modelling approach used in the previous model releases ECHAM3 (Hoffmann et al., 1998) and ECHAM4 (e.g. Werner et al., 2001). For each phase of "normal" water (vapour, cloud liquid, cloud ice) being transported independently in ECHAM5, a corresponding isotopic counterpart is implemented in the model code. The isotopic and the "normal" water are described identically in the GCM as long as no phase transitions are concerned. Therefore, the transport scheme both for active tracers (moisture, cloud liquid water) and for the corresponding passive tracers (moisture, cloud water and cloud ice of the isotopologues) is the flux-form semi-Lagrangian transport scheme for positive definite variables implemented in ECHAM5 (Lin and Rood, 1996). Additional fractionation processes are defined for the water isotopologue variables whenever a phase change of the "normal" water occurs in ECHAM5. Two types of fractionation processes are considered in the model: equilibrium and non-equilibrium processes. An equilibrium fractionation takes place if the corresponding phase change is slow enough to allow full isotopic equilibrium. On the other hand, non-equilibrium processes depend even on the velocity of the phase change, and therefore on the molecular diffusivity of the water isotopologues. Processes which involve fractionation processes include the evaporation from the ocean, condensation either to liquid or to ice, as well as re-evaporation of liquid precipitation within the atmosphere. For evapotranspiration from land surfaces, possible isotopic fractionation is neglected (see Hoffmann et al., 1998 for detailed discussion of this issue).

ECHAM5-wiso has been validated with observations of isotopologue concentrations in precipitation and water vapour (Langebroeck et al., 2011; Werner et al., 2011). On a global and European scale, the annual as well as seasonal ECHAM-5-wiso simulation results are in good agreement with available observations from the Global Network of Isotopes in Precipitation, GNIP (IAEA-WMO, 2006). Furthermore, it has been shown that the simulation of water isotopologues in precipitation does clearly improve for an increased horizontal and vertical model resolution (Werner et al., 2011). The simulated near-surface isotopic composition of atmospheric water vapour δD_v is also in fairly good agreement with recent observations from five different GNIP stations. Model values and measurements agree well with differences in the range of ± 10 ‰. A comparison of the ECHAM5-wiso simulations with total column averaged HDO data determined by the SCIAMACHY instrument on board the environmental satellite ENVISAT (Frankenberg et al., 2009) shows the same latitudinal gradients, but an offset between 20 and 50 ‰ of unknown origin. Focusing on Europe, the results by Langebroeck et al. (2011) indicate that variations of $\delta^{18}O$ in precipitation are rather a regionally integrated signal of several climate variables than a proxy for either local temperature or precipitation changes. This finding is not just valid for ECHAM5-wiso results, but is also supported by other modelling results

(e.g. Schmidt et al., 2005) and confirmed by observational data (GNIP and ERA-40).

Based on our previous findings, we employ in this study the ECHAM5-wiso model with a medium-fine horizontal spectral resolution T63 (about 1.9° × 1.9°). The vertical resolution is 31 hybrid levels. The model is forced with prescribed values of present-day insolation and greenhouse gas concentrations (IPCC, 2000), as well as with sea-surface temperatures and sea-ice concentrations according to ERA-Interim reanalysis data (Dee et al., 2011; Berrisford et al., 2009; ECMWF data server, 2012).

In order to allow a comparison with observations at the sub-seasonal scale, the ECHAM5-wiso model is nudged to reanalysis data, which ensures that the large-scale atmospheric dynamics is correctly represented. Every 6 hours the dynamic–thermodynamic state of the model atmosphere is constrained to observations by implicit nudging (e.g. Krishamurti et al., 1991; implemented by Rast, 2012), i.e. modelled fields of surface pressure, temperature, divergence and vorticity are relaxed to ERA-Interim reanalysis fields (Dee et al., 2011; Berrisford et al., 2009). If we compare climatological means of measured surface temperatures in Yekaterinburg (Russia's Weather Server, 2012) with ERA-40 climatology data, we find a good agreement of the temperature seasonal cycle. The ERA-40 mean monthly surface temperatures show a small warm bias of less than 1 °C for the period May–November, and slightly larger deviations (+1.0 to +2.2 °C) between December and April.

Although the hydrological cycle in our ECHAM5 setup is fully prognostic and not nudged to the ERA-Interim data, in western Siberia the differences of the simulation results as compared to the hydrometeorological reanalysis fields are small. For instance, modelled daily precipitation agrees within 1 mm day^{-1} with reanalysis data, and the agreement with observations further improves if monthly averages are considered. The simulated total column water vapour (TCWV) tends to be systematically overestimated by 4–6 mm compared with reanalysis fields.

Our simulation starts on 1 January 2000, with an internal model time step of 12 min. For comparison with the available isotope observational records at Kourovka, we analyse simulation results for the period April to September 2012. We always evaluate model results with a temporal resolution of 1 hour, if not stated otherwise. For Kourovka, we are using values at the model grid point closest to the station.

For the period April to September 2012, an analysis of ERA-40 and ERA-Interim surface temperature data reveals that the region around Kourovka station was anomalously warm, as compared to the long-time average temperatures (reference period 1960–1999). Strongest above-average warming with temperature anomalies of ≈ +4 °C occurred in April and June, while in May and July temperatures were only about 1–2 °C warmer than average. For August, we find still an above-average warming of 1–2 °C at Kourovka and adjacent regions of western Siberia, but also cooler than average temperatures of the same order of magnitude in large parts of eastern Siberia. For September, temperatures in all Siberian regions were anomalously warm by ≈ 1–3 °C.

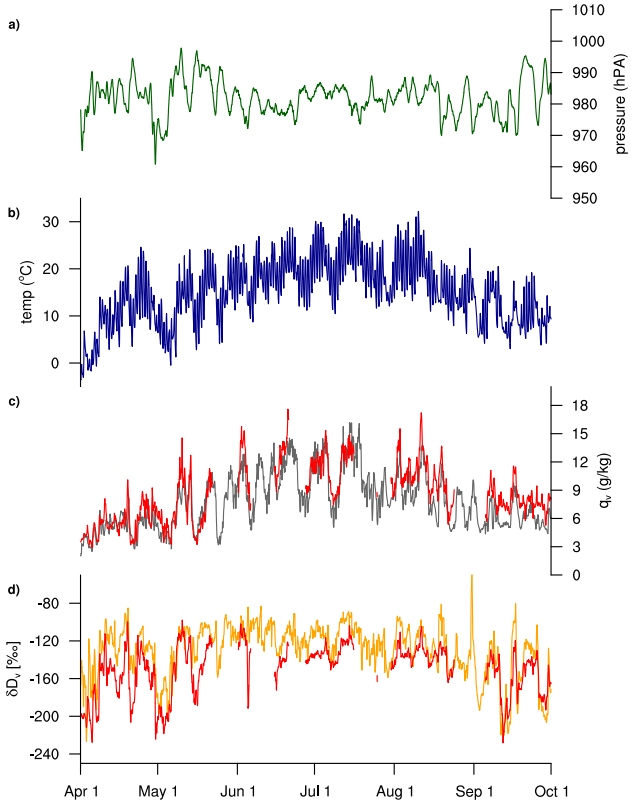

Figure 6. Time series of ECHAM5-wiso simulation values between 1 April and 30 September 2012 of **(a)** surface pressure (green line), **(b)** surface temperature (blue), **(c)** vapour amount q_v of the lowest model grid box (grey), **(d)** δD of the water vapour (yellow). In panel **(c)** and **(d)** the related smoothed PICARRO measurements (red lines) are shown for comparison. The model values are all taken from the grid box enclosing Kourovka station.

4.2 Model results

We briefly describe the simulated near-surface temperature and surface pressure at the location of Kourovka (Fig. 6). A clear diurnal cycle is evidenced with typical day–night temperature changes of ≈ 5–10 °C. Superimposed on this diurnal cycle, the temperature record reveals strong variations within a timescale of a few days. These changes can be as large as 10–15 °C. On the seasonal timescale, the difference between low-temperature values in April and September, respectively, and the summer temperature maximum in mid-July to mid-August adds up to ≈ 20 °C. This is slightly higher than the climatological observations from Yekaterinburg. Surface pressure at Kourovka varies between 960 and 1000 hPa. This record also shows some multi-day variations but clearly lacks both a diurnal and seasonal cycle.

The simulated amount of water vapour q_v in the lowest atmospheric model layer also shows strong temporal variations at a timescale of a few days. While the water content in the air is rather low (3–6 g kg^{-1} air) between the beginning of April and early May, it rises thereafter to values of up to 15 g kg^{-1} air. From mid-July to end of September, the simulated q_v values then fall back into the range 5–10 g kg^{-1} air.

ECHAM5-wiso simulates surface-level water vapour δD_v values (hereafter δD_v) mostly in the range -200 to -100 ‰ at the Kourovka site between April and September 2012 (Fig. 6). The model shows isotopic variations of 30–50 ‰ over a few days, over which are superimposed smaller short-term fluctuations lasting a few hours. The lowest δD_v values are found in early April and early May as well as in mid- to late September, while summer δD_v values are less depleted. A distinct peak event in δD_v occurs between 30 August and 3 September.

Both the simulated δD_v values of the total water vapour column and δD in precipitation (not shown) are highly correlated with the simulated δD_v values near surface ($r = 0.90$ and $r = 0.97$, respectively, for hourly values between 1 April and 30 September). Compared to the surface values, the δD_v signal of total water column is depleted by $\approx$ 20–30 ‰. Precipitation occurs at 1216 1 h intervals between April and September (total number of 1 h intervals during this period: 4392) with a mean enrichment of $\approx$ +70 ‰ as compared to the surrounding vapour.

As seen in Fig. 6, the multi-day variations of δD_v, q_v and surface pressure are strongly correlated. From our analyses, we find the strongest links between variations of temperature and water amount q_v ($r = 0.70$), while variations of δD_v are only weakly linked to local temperature ($r = 0.56$) and q_v ($r = 0.60$). Our results support previous findings that δD_v variations on daily and synoptic timescales are often not strongly correlated with local temperature or water amount changes, but rather represent a more integrated signal of the climatic conditions during the transport of the vapour to a specific site (e.g. Schmidt et al., 2005; Langebroeck et al., 2011). Modelled surface pressure variations at Kourovka are neither strongly correlated to surface temperatures, to water vapour, nor to δD_v (correlation coefficient $|r| < 0.2$ in all cases).

In addition to δD, the isotopic signal of $\delta^{18}O$ of the various water reservoirs and fluxes is also modelled within this ECHAM5-wiso simulation. At the grid point closest to Kourovka, we find a strong linear correlation between hourly values of δD_v and $\delta^{18}O_v$ ($r = 0.997$), with a slope of $m = 7.99$ and a mean deuterium excess value d (defined as $d = \delta D - 8 \times \delta^{18}O$) of +10.2 ‰. Between April and September, the modelled hourly excess values range between +5 ‰ and +20 ‰. The potential use of the deuterium excess data to identify different transport regimes of moisture towards Kourovka will be investigated in detail in future studies.

From correlation analyses (not shown) of the simulated daily mean δD_v values at Kourovka and the isotopic composition at all other grid cells, we estimate that variations of isotope values in vapour at Kourovka are representative for isotopic changes in a region between 45–75° E and 48–66° N, with a correlation coefficient r higher than +0.5. A similar correlation pattern is found for variations of the water vapour amount q, but with slightly higher mean correlation coefficients ($r \geq +0.65$). In contrast to these water quantities, the simulated near-surface temperature shows a much stronger and spatially extended correlation between Kourovka and its surroundings (mean r values > 0.9).

5 Data comparison

5.1 Surface δD_v: model data comparison

The ECHAM5-wiso results are first compared to the observed hourly water vapour PICARRO data q_v (Fig. 3c, red lines). The model correctly captures the patterns and magnitude of variability, with a very large correlation coefficient ($r = 0.89$). Absolute values of water vapour measured with the PICARRO instrument are up to 20 % higher than the related model values. This might be explained by the facts that the ECHAM5-wiso values represent the mean of the lowest atmospheric model level (surface to $\approx$ 60 m) while the PICARRO measurements were carried out at a height of 8 m, and that the closest model grid box has a much larger size than the point of in situ measurements and is located above complicated terrain containing small lakes and rivers with altitude differences of about 400 m.

Simulated δD_v values are often 30–40 ‰ less depleted than the corresponding PICARRO data. This suggests a lack of depletion either along air mass trajectories or due to boundary layer mixing. Despite the systematic offset, a high correlation ($r = 0.77$) is obtained between model and observed δD_v hourly variations. This result shows that the intra-seasonal δD_v variability at Kourovka is dominated by the synoptic variability, which is correctly resolved by the model in the nudged configuration.

The PICARRO data exhibit a stronger correlation between δD_v and q_v ($r = 0.73$) than simulated ($r = 0.60$). We note that this might be partly influenced by the lower number of measured data points ($n = 3066$) as compared to the total number of hourly modelled values ($n = 4392$) available for the period between April and September 2012. However, if we limit the analyses of the ECHAM5 values to those points in time when PICARRO measurements exist, the simulated correlation between δD_v and q_v strengthens only slightly ($r = 0.61$).

The PICARRO observations and ECHAM5-wiso results consistently depict two pronounced δD_v negative excursions with minimum and maximum values of -200 and -100 ‰, respectively, for the first days of April 2012 and May 2012. Another negative excursion occurs on 12 September. Exemplarily, we have chosen the May event with highly depleted

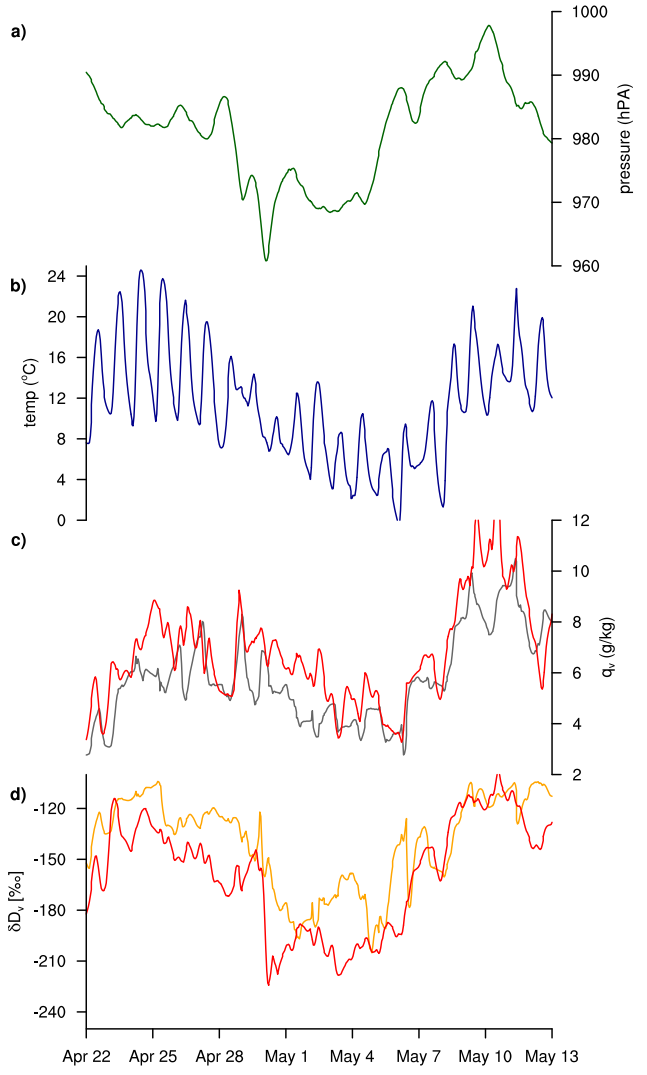

Figure 7. The same as Fig. 6, but for the period 22 April to 13 May.

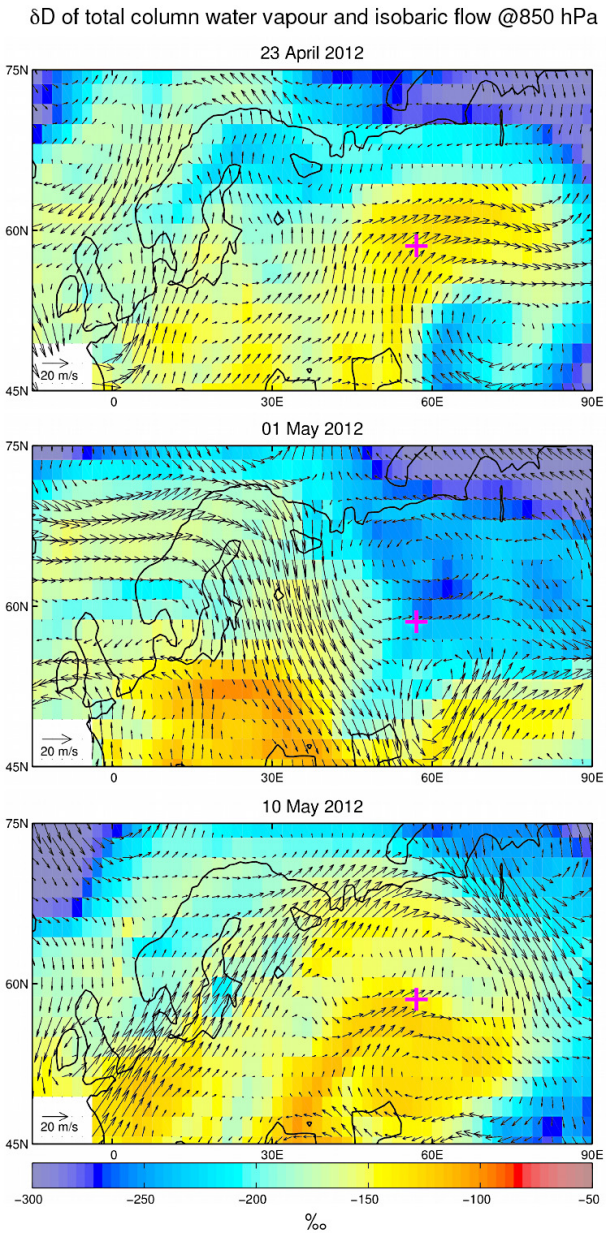

Figure 8. Horizontal wind flow at 850 hPa (vectors) and δD composition of the total water column (coloured pattern) for **(a)** 23 April, **(b)** 1 May, **(c)** 10 May for the region 45–75° N, 15° W–90° E as simulated by ECHAM5-wiso. The location of Kourovka station is marked by a red cross.

δD_v values between end of April and early May for a detailed analysis of the atmospheric conditions leading to this fast and strong isotope shift in vapour at Kourovka (Fig. 7). In the model framework, the minimum in δD_v lags a local surface pressure minimum by 1 day and precedes a drop in surface air temperature, which reaches its lowest temperatures 4 days later. This sequence of events suggests that such δD_v variations at Kourovka are related to passages of dynamic low- and high-pressure systems and advection of remote air masses. This hypothesis is further investigated by analysis of the isobaric flow at 850 hPa. A few days before this depletion event, the Kourovka area was receiving southwesterly air masses transporting relatively warm and enriched vapour (Fig. 8, top panel). Around 1 May, the atmospheric circulation changed due to a pronounced low-pressure system north of Kourovka. As a result, the main air flow was then transported from central Siberia with depleted δD_v levels (Fig. 8, middle panel). During the following days, this northerly airflow caused the cooling at Kourovka. Starting from 7 May, a new high-pressure system south of Kourovka was again dominating the atmospheric flow pattern, bringing warm and relatively enriched vapour to this region (Fig. 8, bottom panel). These simulated changes in atmospheric transport to Kourovka between 20 April and 11 May are in good agreement with back-trajectory analyses of air masses, available

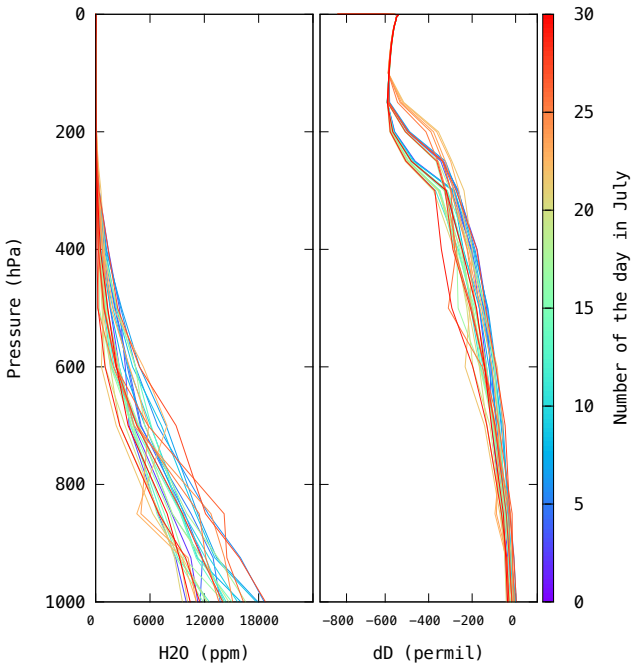

Figure 9. H_2O and corresponding δD a priori profiles derived from NCEP/NCAR reanalysis data using Eq. (1).

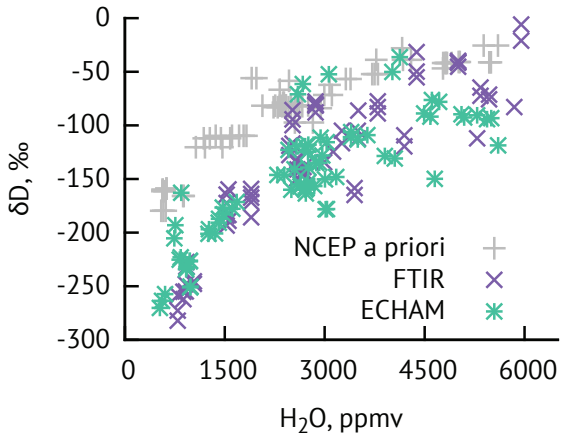

Figure 10. H_2O vs. δD plots from a priori for FTIR retrieval, FTIR retrievals, and ECHAM5-wiso data. Most of the retrieved δD variations are already accounted for by the a priori states.

from the AERONET (2012) for the location of Yekaterinburg (not shown).

We conclude that PICARRO measurements and ECHAM5-wiso simulation results of δD_v and related quantities (vapour q, surface temperature) between April and September 2012 are in good agreement. Even short-term isotope variations occurring on an hourly timescale are correctly reproduced in this nudged simulation. Thus, one may safely use the ECHAM5-wiso model results for an improved interpretation of observed isotopic variations near Kourovka in future studies.

5.2 Comparison of FTIR data with measured at surface and model data

Since the model provides hourly averaged output data, data retrieved from FTIR measurements taken within 1 h were also averaged. For the comparison between model and FTIR observations we assume that the modelled HDO and H_2O profiles are true, and we smooth original model values by applying the following equation (Rodgers and Connor, 2003; Risi et al., 2012a; Wunch et al., 2010):

$$Q = \sum_{i=1}^{n} \frac{\Delta P_i}{g} \left(A_i \cdot q_i^{\mathrm{sim}} + (1 - A_i) \cdot \gamma q_i^{\mathrm{apr}} \right), \qquad (2)$$

where γ is the retrieved scaling factor for the a priori profile. Here, Q is the retrieved total column mass of HDO or H_2O, respectively, q^{sim} is the specific humidity profile simulated by the model for atmospheric layer i, q^{apr} is the specific humidity in the same layer according to the a priori profile used in the retrieval (converted from wet to dry-mole fractional values according to Wunch et al., 2010), A_i is the ith component of the column averaging kernel vector, ΔP_i is the thickness of the ith atmospheric layer, g is the gravity acceleration. Column averaging kernel as a function of pressure for different solar zenith angles of measurements are shown in Fig. 11. GFIT a priori and averaging kernel profiles are tabulated using a different vertical coordinate system than the model profiles (71 pressure levels vs. 31 hybrid layers). To ensure numerical consistency, model profiles were interpolated to the same vertical resolution as averaging kernel (71 pressure levels) before the vertical integration was carried out. The $\delta D_v^{\mathrm{FTIR}}$ of total column water vapour (δD_{TCVW}) was then calculated from the normalized ratio of Q_{HDO} and Q_{H_2O}.

To check how retrieved columnar $\delta D_v^{\mathrm{FTIR}}$ values correlate to collocated ground δD_v values we selected FTIR and extended until June 2013 PICARRO measurements taken within the same hours.

Before we enter the comparison between smoothed ECHAM5-wiso results and observations, we consider the effect of applying column-averaging kernels to the original model results. In Kourovka, it shifts the original model results for δD_{TCVW} to more positive values by about 32 ‰ in the average, and also induces a change of the expected slope between smoothed and originally simulated δD_{TCVW} from 1.0 to 0.78. The positive shift of retrieval values is essentially a consequence of the fact that between 1000 and 200 hPa, the isotopic ratio of TCCON a priori profiles is systematically higher than in the ECHAM simulations. The change of the slopes deserves further investigation.

FTIR measurements were carried out in Kourovka on 32 days during one year between 10 July 2012 and 30 June 2013. To evaluate whether HDO retrievals add some

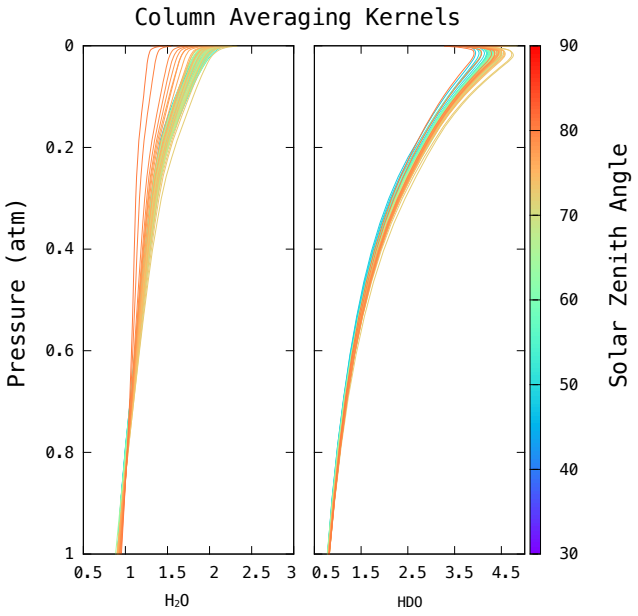

Figure 11. H_2O and HDO column averaging kernels for different solar zenith angles.

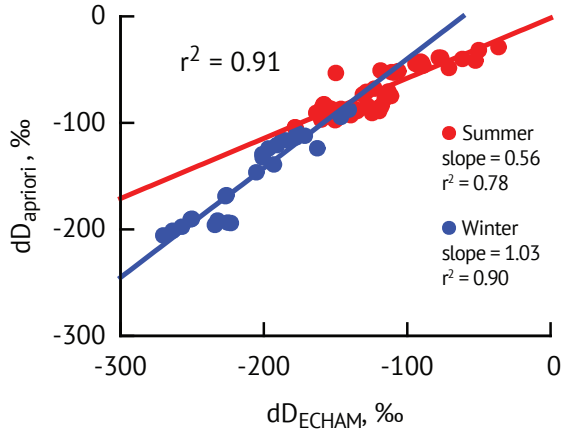

Figure 12. Winter and summer δD calculated from retrieved H_2O using Eq. (1) vs. ECHAM5-wiso output without FTIR retrieval of HDO.

value to information on δD in the atmosphere, we compared a priori δD calculated from retrieved H_2O using Eq. (1) (denoted as $\delta D_{a\ priori}$, because it does not contain information from HDO retrieval) to ECHAM5-wiso output. Also we divided all measurements into summer data (air temperature at surface is above 15°C) and winter data (temperature is below −15°C). As one can see in Fig. 12, a priori and simulated data are already in good agreement with $r^2 = 0.91$, and winter values are in better agreement with the model data than summer data.

The values of δD_v^{FTIR} obtained from retrieved H_2O and HDO concentrations range from −282 ‰ on 22 February 2013 to −5.9 ‰ on 12 June 2013. Multiple measure-

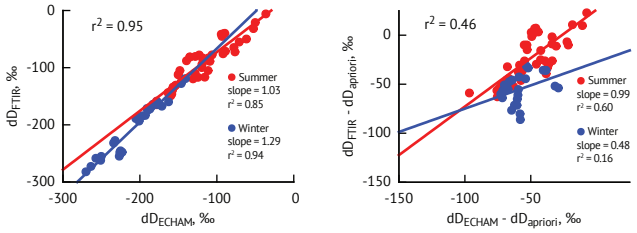

Figure 13. FTIR results comparison: (left panel) with columnar ECHAM5-wiso δD_v values and (right panel) with subtraction of all a priori variations.

ments on July 10, 2012 record an increase of δD_v^{FTIR} from morning to noon by about 15 ‰. Observations and smoothed model results are correlated with $r^2 = 0.95$ and scatter with an absolute standard deviation of 19 ‰ (see Fig. 13a). The observations are systematically shifted to the higher values compared to the model results by approximately 18 ‰ and have larger amplitude of variations by approximately 30 %. Systematic shift and slope in results can be explained by the uncertainties in spectroscopic parameters, such as line intensities, broadening and temperature dependence of broadening coefficient in the line list. The measured increase of δD_v^{FTIR} since 10 July 2012 is also found in the model results but with a smaller amplitude (10 ‰). In the model, this fast isotopic enrichment coincides with the temporal evolution of lower tropospheric temperatures, exhibiting for Kourovka a pronounced diurnal cycle during the summer months. The values of δD_v^{FTIR} demonstrate better agreement with the model than the values of $\delta D_{a\ priori}$, especially for summer months. Hence, FTIR retrievals add some information to our knowledge of δD distribution in the atmosphere. While correlation for winter measurements is improved after retrieval of HDO from FTIR measurements, the slope has deteriorated. Fig. 13b represents δD_v^{FTIR} compared to ECHAM5-wiso output – both values are with the deduction of $\delta D_{a\ priori}$ which includes contribution from NCEP/NCAR reanalysis data, H_2O variations, and dependence of HDO on H_2O corresponding to Eq. (1). Bad correlation between winter values can be conditioned by low spectral signal because of low concentration of H_2O in cold air. The correlations between columnar and measured at surface values of δD_v were also investigated. The left panel of Fig. 14 shows columnar vs. surface values from ECHAM5-wiso output. For this plot we used smoothed values calculated using Eq. (2) as columnar values and lowest point in model vertical profiles as surface values. The right panel of Fig. 14 shows FTIR columnar retrieved values vs. values measured by Picarro instrument at the surface; all data are hourly averaged. This comparison demonstrates that correlations for both cases are approximately the same ($r = 0.68$ vs. $r = 0.63$ for summer, and $r = 0.80$ vs. $r = 0.82$ for winter).

Study of the influence of different sources of uncertainties on δD_v retrieved from near-infrared solar spectra measured at

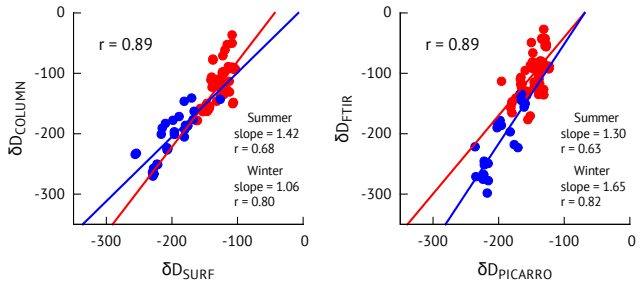

Figure 14. Comparison of columnar δD_v vs. δD_v at surface: ECHAM5-wiso averaged using Eq. (2) δD_v vs. ECHAM5-wiso δD_v at surface (left panel), and FTIR retrievals compared to δD_v measured by Picarro instrument at surface (right panel).

the surface and more detailed investigation of retrieval sensitivity and cross-dependence on humidity is postponed for the future.

6 Conclusions

The present study is part of a project aiming to investigate the water and carbon cycles in permafrost regions and pristine peatlands of western Siberia and their projected changes under a warming climate. The isotopic approach is a key element of this project and the results that we have presented and discussed should be considered as a first and necessary step to fully exploit the isotopic information contained in water vapour. To this end we have combined two independent methods to acquire data (continuous surface measurements and FTIR) and evaluate them against the results derived from a dedicated simulation of the ECHAM5-wiso IGCM focusing on this region.

As expected from a Rayleigh type model, and generally observed in middle- and high-latitude regions (Rozanski et al., 1992), a significant part of the daily isotopic variations (δD_v) observed in Kourovka water vapour is explained by local changes in the amount of water vapour ($r^2 = 0.71$) and temperature ($r^2 = 0.72$). Obviously, a general circulation model which accounts for the origin of the water vapour, for the complexity of weather situations and for the differences of associated fractionations (e.g convective vs. non-convective systems) is a more appropriate tool to examine the link between δD_v and climatic parameters. There is indeed an excellent correlation between observed and predicted δD_v values including for rapid excursions related to concurrent changes in atmospheric circulation.

This data model comparison fully justifies the use of ECHAM5-wiso to evaluate the method based on the exploitation of FTIR data, allowing remote measurements of δD_v in the water column. The method is very satisfying despite being limited to a small number of days. At the same time, further comparison of model simulations with δD_v retrievals at FTIR stations (including TCCON sites) is necessary.

To sum up, the δD_v comparison between two observational approaches and a medium–high resolution IGCM, undertaken for the first time at a given site, is quite promising. Data acquisition with the Picarro instrument will now be performed on a continuous basis and a second instrument will be deployed in summer 2013 at Labytnangi located near the Arctic circle (66° 39′ N, 66° 23′ E, see Fig. 1) with the aim of contributing to an Arctic network now under development. Further work will include the exploitation of oxygen-18 and associated deuterium excess from the PICARRO data, a comparison of the algorithm developed to infer column δD_v from the GOSAT thermal infrared band and the method currently applied in the short-wave infrared (Frankenberg et al., 2012), as well as the development of an improved algorithm to exploit FTIR data for isotopic purposes. A comprehensive theoretical study for characterization of near-infrared δD_v ground-based FTIR product is required. Finally, the use of a second IGCM (LMDZiso) together with cloud-resolving models with isotopic water precipitations (Blossey et al. , 2010) should help to interpret these data in a larger geographical context.

Acknowledgements. This research was supported by a grant of Russian government under contract 11.G34.31.0064 and RFBR grant no. 12-01-00801-a. We acknowledge H. C. Steen-Larsen for fruitful discussions on measurements techniques and calibrations, and M. Schneider for fruitful discussions on a posteriori calculations of δD using H_2O and HDO retrievals in the near-infrared. V. I. Zakharov and N. V. Rokotyan thank I. Ptashnik for fruitful discussions regarding the impact of error of spectral parameters of target molecules on precision of the retrieval and his suggestion to use the revised water line list.

Edited by: M. K. Dubey

References

Aerosol Robotic Network (AERONET): http://aeronet.gsfc.nasa.gov/new_web/index.html, last access: 1 July 2012.

Berrisford, P., Dee, D., Fielding, K., Fuentes, M., Kallberg, P., Kobayashi, S., and Uppala, S.: The ERA-Interim archive, ERA Report Series, European Centre for Medium Range Weather Forecast, Shinfield Park, Reading, Berkshire RG29AX, United Kingdom, August 2009, 2009.

Blossey, P. N., Kuang, Z., and Romps, D. M.: Isotopic composition of water in the tropical tropopause layer in cloud-resolving simulations of an idealized tropical circulation, J. Geophys. Res., 115, D24309, doi:10.1029/2010JD014554, 2010.

Boesch, H., Deutscher, N. M., Warneke, T., Byckling, K., Cogan, A. J., Griffith, D. W. T., Notholt, J., Parker, R. J., and Wang, Z.: HDO / H_2O ratio retrievals from GOSAT, Atmos. Meas. Tech., 6, 599–612, doi:10.5194/amt-6-599-2013, 2013.

Brand, W. A.: Maintaining high precision of isotope ratio analysis over extended periods of time, Isot. Environ. Health S., 45, 135–149, 2009.

Craig, H.: Standard for reporting concentrations of deuterium and oxygen-18 in natural waters, Science, 133, 1833–1834, 1961.

Dansgaard, W.: Stable isotopes in precipitation, Tellus, 16, 436–468, doi:10.1111/j.2153-3490.1964.tb00181.x, 1964.

Dee, D. P., Uppala, S. M., Simmons, A. J., Berrisford, P., Poli, P., Kobayashi, S., Andrae, U., Balmaseda, M. A., Balsamo, G., Bauer, P., Bechtold, P., Beljaars, A. C. M., van de Berg, L., Bidlot, J., Bormann, N., Delsol, C., Dragani, R., Fuentes, M., Geer, A. J., Haimberger, L., Healy, S. B., Hersbach, H., Hólm, E. V., Isaksen, L., Kållberg, P., Köhler, M., Matricardi, M., McNally, A. P., Monge-Sanz, B. M., Morcrette, J.-J., Park, B.-K., Peubey, C., de Rosnay, P., Tavolato, C., Thépaut, J.-N., and Vitart, F.: The ERA-Interim reanalysis: configuration and performance of the data assimilation system, Q. J. Roy. Meteor. Soc., 137, 553–597, 2011.

ECMWF data server: http://data-portal.ecmwf.int/ (last access: 30 September 2012), 2012.

Frankenberg, C., Yoshimura, K., Warneke, T., Aben, I., Butz, A., Deutscher, N., Griffith, D., Hase, F., Notholt, J., Schneider, M., Schrijver, H., and Röckmann, T.: Dynamic processes governing lower-tropospheric HDO/H_2O ratios as observed from space and ground, Science, 325, 1374–1377, 2009.

Frankenberg, C., Wunch, D., Toon, G., Risi, C., Scheepmaker, R., Lee, J.-E., Wennberg, P., and Worden, J.: Water vapor isotopologues retrievals from high resolution GOSAT short-wave infrared spectra, Atmos. Meas. Tech. Discuss., 5, 6357-6386, doi:10.5194/amtd-5-6357-2012, 2012.

Frankenberg, C., Wunch, D., Toon, G., Risi, C., Scheepmaker, R., Lee, J.-E., Wennberg, P., and Worden, J.: Water vapor isotopologue retrievals from high-resolution GOSAT shortwave infrared spectra, Atmos. Meas. Tech., 6, 263–274, doi:10.5194/amt-6-263-2013, 2013.

Gupta, P., Noone, D., Galewsky, J., Sweeney, C., and Vaughn, B. H.: Demonstration of high-precision continuous measurements of water vapor isotopologues in laboratory and remote field deployments using wavelength-scanned cavity ring-down spectroscopy (WS-CRDS) technology, Rapid Commun. Mass Sp., 23, 2534–2542, 2009.

Hagemann, S., Arpe, K., and Roeckner, E.: Evaluation of the hydrological cycle in the ECHAM5 model, J. Climate, 19, 3810–3827, 2006.

Hannigan, J. W., Coffey, M. T., and Goldman, A.: Semi-autonomous FTS ObservaLon system for remote sensing of stratospheric and tropospheric gases, J. Atmos. Ocean Tech., 26, 1814–1828, doi:10.1175/2009JTECHA1230.1, 2009.

Herbin, H., Hurtmans, D., Clerbaux, C., Clarisse, L., and Coheur, P.-F.: H216O and HDO measurements with IASI/MetOp, Atmos. Chem. Phys., 9, 9433–9447, doi:10.5194/acp-9-9433-2009, 2009.

Hoffmann, G., Werner, M., and Heimann, M.: Water isotope module of the ECHAM atmospheric general circulation model: a study on timescales from days to several years, J. Geophys. Res., 103, 16871–16896, 1998.

IAEA-WMO, Global Network of Isotopes in Precipitation: The GNIP Database: http://www-naweb.iaea.org/napc/ih/IHS_resources_gnip.html (last access: 20 December 2012), 2006.

Joussaume, S., Sadourny, R., and Jouzel, J.: A general circulation model of water isotope cycles in the atmosphere, Nature, 311, 24–29, 1984.

Jouzel, J., Russell, G. L., Suozzo, R. J., Koster, R. D., White, J. W. C., and Broecker, W. S.: Simulations of the HDO and $H_2^{18}O$ atmospheric cycles using the NASA GISS General Circulation Model: the seasonal cycle for present-day conditions, J. Geophys. Res., 92, 14739–14760, 1987.

Kalnay, E., Kanamitsu, M., Kistler, R., Collins, W., Deaven, D., Gandin, L., Iredell, M., Saha, S., White, G., Woollen, J., Zhu, Y., Leetmaa, A., and Reynolds, R.: The NCEP/NCAR 40-year reanalysis project, B. Am. Meteorol. Soc., 77, 437–471, 1996.

Krishnamurti, T. N., Xue, J., Bedi, H. S., Ingles, K., and Oosterhof, D.: Physical initialization for numerical weather prediction over the tropics, Tellus, 43, 53–81, 1991.

Lacour, J.-L., Risi, C., Clarisse, L., Bony, S., Hurtmans, D., Clerbaux, C., and Coheur, P.-F.: Mid-tropospheric δD observations from IASI/MetOp at high spatial and temporal resolution, Atmos. Chem. Phys., 12, 10817–10832, doi:10.5194/acp-12-10817-2012, 2012.

Langebroeck, P. M., Werner, M., and Lohmann, G.: Climate information imprinted in oxygen-isotopic composition of precipitation in Europe, Earth Planet. Sc. Lett., 311, 144–154, 2011.

Lin, S.-J. and Rood, R. B.: Multidimensional flux-form semi-Lagrangian transport schemes, Mon. Weather Rev., 124, 2046–2070, 1996.

Lossow, S., Steinwagner, J., Urban, J., Dupuy, E., Boone, C. D., Kellmann, S., Linden, A., Kiefer, M., Grabowski, U., Glatthor, N., Höpfner, M., Röckmann, T., Murtagh, D. P., Walker, K. A., Bernath, P. F., von Clarmann, T., and Stiller, G. P.: Comparison of HDO measurements from Envisat/MIPAS with observations by Odin/SMR and SCISAT/ACE-FTS, Atmos. Meas. Tech., 4, 1855–1874, doi:10.5194/amt-4-1855-2011, 2011.

Nakicenovic, N. and Swart, R. (Eds.): IPCC Special Report on Emissions Scenarios, IPCC, Cambridge University Press, Cambridge, UK, 2000.

Nassar, R., Bernath, P. F., Boone, C. D., Gettelman, A., McLeod, S. D., and Rinsland, C. P.: Variability in HDO/H_2O abundance ratios in the tropical tropopause layer, J. Geophys. Res., 112, D21305, doi:10.1029/2007JD008417, 2007.

Notholt, J. and Schrems, O.: Ground-based FTIR measurements of vertical column densities of several trace gases above Spitsbergen, Geophys. Res. Lett., 21, 1355–1358, 1994.

Payne, V. H., Noone, D., Dudhia, A., Piccolo, C., and Grainger, R. G.: Global satellite measurements of HDO and implications for understanding the transport of water vapour into the, Q. J. Roy. Meteor. Soc., 133, 1459–1471, doi:10.1002/qj.127, 2007.

Petri, C.: Ground-based remote sensing of CO_2 and CH_4 using a Bruker 120/5 M FTS, IRWG/TCCON meeting, Wengen, Switzerland, 11–15 June 2012, 2012.

Rast, S.: Sea ice and nudging in ECHAM5, available at: http://www.mpimet.mpg.de/en/staff/sebastian-rast/echam-special-documentation.html, last access: 8 December 2012.

Risi, C., Noone, D., Worden, J., Frankenberg, C., Stiller, G., Kiefer, M., Funke, B., Walker, K., Bernath, P., Schneider, M., Wunch, D., Sherlock, V., Deutscher, N., Griffith, D., Wennberg, P. O., Strong, K., Smale, D., Mahieu, E., Barthlott, S., Hase, F., García, O., Notholt, J., Warneke, T., Toon, G., Sayres, D., Bony, S., Lee, J., Brown, D., Uemura, R., and Sturm, C.: Process-evaluation of tropospheric humidity simulated by general cir-

culation models using water vapor isotopologues: 1. Comparison between models and observations, J. Geophys. Res., 117, D05303, doi:10.1029/2011JD016621, 2012a.

Risi, C., Noone, D., Worden, J., Frankenberg, C., Stiller, G., Kiefer, M., Funke, B., Walker, K., Bernath, P., Schneider, M. Bony, S., Lee, J., Brown, D., and Sturm, C.: Process-evaluation of tropospheric humidity simulated by general circulation models using water vapor isotopic observations: 2. Using isotopic diagnostics to understand the mid and upper tropospheric moist bias in the tropics and subtropics, J. Geophys. Res., 117, D05304, doi:10.1029/2011JD016623, 2012b.

Rodgers, C. D. and Connor, B. J.: Intercomparison of remote sounding instruments, J. Geophys. Res., 108, 4116, doi:10.1029/2002JD002299, 2003.

Roeckner, E., Bäuml, G., Bonaventura, L. Brokopf, R., Esch, M., Giorgetta, M., Hagemann, S., Kirchner, I., Kornblueh, L., Manzini, E., Rhodin, A., Schlese, U., Schulzweida, U., and Tompkins, A.: The atmospheric general circulation model ECHAM5, Part 1, Model description, Report No. 349, Max Planck Institute for Meteorology, Hamburg, Germany, 2003.

Roeckner, E., Brokopf, R., Esch, M., Giorgetta, M., Hagemann, S., Manzini, E., Schlese, U., and Schulzweida, U.: Sensitivity of simulated climate to horizontal and vertical resolution in the ECHAM5 atmosphere model, J. Climate, 19, 3771–3791, 2006.

Rothman, L. S., Gordon, I. E., Barbe, A., Benner, D., Chris, Bernath, P. F., Birk, M., Boudon, V., Brown, L. R., Campargue, A., Champion, J.-P., Chance, K., Coudert, L. H., Dana, V., Devi, V. M., Fally, S., Flaud, J.-M., Gamache, R. R., Goldman, A., Jacquemart, D., Kleiner, I., Lacome, N., Lafferty, W. J., Mandin, J.-Y., Massie, S. T., Mikhailenko, S. N., Miller, C. E., Moazzen-Ahmadi, N., Naumenko, O. V., Nikitin, A. V., Orphal, J., Perevalov, V. I., Perrin, A., Predoi-Cross, A., Rinsland, C. P., Rotger, M., Šimeèková, M., Smith, M. A. H., Sung, K., Tashkun, S. A., Tennyson, J., Toth, R. A., Vandaele, A. C., and Vander Auwera, J.: The HITRAN 2008 molecular spectroscopic database., J. Quant. Spectros. Ra., 110, 533–572, doi:10.1016/j.jqsrt.2009.02.013, 2009.

Rozanski, K., Araguás-Araguás, L., and Gonfiantini, R.: Relation between long-term trends of oxygen-18 isotope composition of precipitation and climate, Science, 258, 981–985, 1992.

Russia's Weather Server – Weather Archive: http://meteo.infospace.ru/wcarch/html/index.sht, last access: 1 December 2012.

Schmidt, G. A., Hoffmann, G., Shindell, D. T., and Hu, Y.: Modeling atmospheric stable water isotopes and the potential for constraining cloud processes and stratosphere-troposphere water exchange, J. Geophys. Res., 110, D21314, doi:10.1029/2005JD005790, 2005.

Schneider, M. and Hase, F.: Optimal estimation of tropospheric H_2O and δD with IASI/METOP, Atmos. Chem. Phys., 11, 11207–11220, doi:10.5194/acp-11-11207-2011, 2011.

Schneider, M., Hase, F., and Blumenstock, T.: Ground-based remote sensing of HDO / H_2O ratio profiles: introduction and validation of an innovative retrieval approach, Atmos. Chem. Phys., 6, 4705–4722, doi:10.5194/acp-6-4705-2006, 2006.

Schneider, M., Toon, G. C., Blavier, J.-F., Hase, F., and Leblanc, T.: H_2O and δD profiles remotely-sensed from ground in different spectral infrared regions, Atmos. Meas. Tech., 3, 1599–1613, doi:10.5194/amt-3-1599-2010, 2010a.

Schneider, M., Sepúlveda, E., García, O., Hase, F., and Blumenstock, T.: Remote sensing of water vapour profiles in the framework of the Total Carbon Column Observing Network (TCCON), Atmos. Meas. Tech., 3, 1785–1795, doi:10.5194/amt-3-1785-2010, 2010b.

Schneider, M., Barthlott, S., Hase, F., González, Y., Yoshimura, K., García, O. E., Sepúlveda, E., Gomez-Pelaez, A., Gisi, M., Kohlhepp, R., Dohe, S., Blumenstock, T., Wiegele, A., Christner, E., Strong, K., Weaver, D., Palm, M., Deutscher, N. M., Warneke, T., Notholt, J., Lejeune, B., Demoulin, P., Jones, N., Griffith, D. W. T., Smale, D., and Robinson, J.: Ground-based remote sensing of tropospheric water vapour isotopologues within the project MUSICA, Atmos. Meas. Tech., 5, 3007–3027, doi:10.5194/amt-5-3007-2012, 2012.

Shalaumova,Yu. V., Fomin, V. V., and Kapralov, D. S.: Spatiotemporal dynamics of the Urals climate in the second half of the 20th century, Russ. Meteorol. Hydrol., 35, 107–114, 2010.

Shillings, A. J. L., Ball, S. M., Barber, M. J., Tennyson, J., and Jones, R. L.: An upper limit for water dimer absorption in the 750 nm spectral region and a revised water line list, Atmos. Chem. Phys., 11, 4273–4287, doi:10.5194/acp-11-4273-2011, 2011.

Steen-Larsen, H. C., Masson-Delmotte, V., Sjolte, J., Johnsen, S. J., Vinther, M. B., Bréon, F.-M., Clausen, H. B., Dahl-Jensen, D., Falourd, S., Fettweis, X., Gallee, H., Jouzel, J., Kageyama, M., Lerche, H., Minster, B., Picard, G., Punge, H. J., Risi, C., Salas, D., Schwander, J., Steffen, K., Sveinbjornsdottir, A. E., Svensson, A., and White, J.: Understanding the climatic signal in the water stable isotope records from the NEEM shallow firn/ice cores in northwest Greenland, J. Geophys. Res.-Atmos., 116, D06108, doi:10.1029/2010JD014311, 2011.

Steen-Larsen, H. C., Johnsen, S. J., Masson-Delmotte, V., Stenni, B., Risi, C., Sodemann, H., Balslev-Clausen, D., Blunier, T., Dahl-Jensen, D., Ellehøj, M. D., Falourd, S., Grindsted, A., Gkinis, V., Jouzel, J., Popp, T., Sheldon, S., Simonsen, S. B., Sjolte, J., Steffensen, J. P., Sperlich, P., Sveinbjörnsdóttir, A. E., Vinther, B. M., and White, J. W. C.: Continuous monitoring of summer surface water vapor isotopic composition above the Greenland Ice Sheet, Atmos. Chem. Phys., 13, 4815–4828, doi:10.5194/acp-13-4815-2013, 2013.

Steinwagner, J., Milz, M., von Clarmann, T., Glatthor, N., Grabowski, U., Höpfner, M., Stiller, G. P., and Röckmann, T.: HDO measurements with MIPAS, Atmos. Chem. Phys., 7, 2601–2615, doi:10.5194/acp-7-2601-2007, 2007.

Tremoy, G., Vimeux, F., Mayaki, S., Souley, I., Cattani, O., Risi, C., Favreau, G., and Oi, M.: A 1-year long $\delta^{18}O$ record of water vapor in Niamey (Niger) reveals insightful atmospheric processes at different timescales, Geophys. Res. Lett., 39, L08805, doi:10.1029/2012GL051298, 2012.

Werner, M., Heimann, M., and Hoffmann, G.: Isotopic composition and origin of polar precipitation in present and glacial climate simulations, Tellus B, 53, 53–71, 2001.

Werner, M., Langebroek, P. M., Carlsen, T., Herold, M., and Lohmann, G.: Stable water isotopes in the ECHAM5 general circulation model: toward high-resolution isotope modeling on a global scale, J. Geophys. Res., 16, D15109, doi:10.1029/2011JD015681, 2011.

Worden, J., Bowman, K., Noone, D., Beer, R., Clough, S., Eldering, A., Fisher, B., Goldman, A., Gunson, M., Her-

man, R., Kulawik, S. S., Lampel, M., Luo, M., Osterman, G., Rinsland, C., Rodgers, C., Sander, S., Shephard, M., and Worden, H.: Tropospheric emission spectrometer observations of the tropospheric HDO/H_2O ratio: estimation approach and characterization, J. Geophys. Res.-Atmos., 111, D16309, doi:10.1029/2005jd006606, 2006.

Worden, J., Noone, D., Galewsky, J., Bailey, A., Bowman, K., Brown, D., Hurley, J., Kulawik, S., Lee, J., and Strong, M.: Estimate of bias in Aura TES HDO / H_2O profiles from comparison of TES and in situ HDO / H_2O measurements at the Mauna Loa observatory, Atmos. Chem. Phys., 11, 4491–4503, doi:10.5194/acp-11-4491-2011, 2011.

Wunch, D., Toon, G. C., Wennberg, P. O., Wofsy, S. C., Stephens, B. B., Fischer, M. L., Uchino, O., Abshire, J. B., Bernath, P., Biraud, S. C., Blavier, J.-F. L., Boone, C., Bowman, K. P., Browell, E. V., Campos, T., Connor, B. J., Daube, B. C., Deutscher, N. M., Diao, M., Elkins, J. W., Gerbig, C., Gottlieb, E., Griffith, D. W. T., Hurst, D. F., Jiménez, R., Keppel-Aleks, G., Kort, E. A., Macatangay, R., Machida, T., Matsueda, H., Moore, F., Morino, I., Park, S., Robinson, J., Roehl, C. M., Sawa, Y., Sherlock, V., Sweeney, C., Tanaka, T., and Zondlo, M. A.: Calibration of the Total Carbon Column Observing Network using aircraft profile data, Atmos. Meas. Tech., 3, 1351–1362, doi:10.5194/amt-3-1351-2010, 2010.

Wunch, D., Toon, G. C., Blavier, J.-F. L., Washenfelder, R. A., Notholt, Connor, B. J., Griffith, D. W. T., Sherlock, V., and Wennberg, P. O.: The total carbon column observing network, Philos. T. Roy. Soc. A, 369, 2087–2112, doi:10.1098/rsta.2010.0240, 2011.

Zakharov, V. I., Imasu, R., Gribanov, K. G., Hoffmann, G., and Jouzel, J.: Latitudinal distribution of the deuterium to hydrogen ratio in the atmospheric water vapor retrieved from IMG/ADEOS data, Geophys. Res. Lett., 31, L12104, doi:10.1029/2004GL019433, 2004.